ARTICLES
PUBLISHED ONLINE: 5 JUNE 2017 | DOI: 10.1038/NPHYS4148
nature physics

Direct measurement of polariton–polariton interaction strength

Yongbao Sun[1]*, Yoseob Yoon[1], Mark Steger[2], Gangqiang Liu[2], Loren N. Pfeiffer[3], Ken West[3], David W. Snoke[2]* and Keith A. Nelson[1]

Exciton–polaritons in a microcavity are composite two-dimensional bosonic quasiparticles, arising from the strong coupling between confined light modes in a resonant planar optical cavity and excitonic transitions. Quantum phenomena such as Bose–Einstein condensation, superfluidity, quantized vortices, and macroscopic quantum states have been realized at temperatures from tens of kelvin up to room temperatures. Crucially, many of these effects of exciton–polaritons depend on the polariton–polariton interaction strength. Despite the importance of this parameter, it has been difficult to make an accurate experimental measurement, mostly because of the difficulty in determining the absolute densities of polaritons and bare excitons. Here we report a direct measurement of the polariton–polariton interaction strength in a very high-Q microcavity structure. By allowing polaritons to propagate over 20 μm to the centre of a laser-generated annular trap, we are able to separate the polariton–polariton interactions from polariton–exciton interactions. The interaction strength is deduced from the energy renormalization of the polariton dispersion as the polariton density is increased, using the polariton condensation as a benchmark for the density. We find that the interaction strength is about two orders of magnitude larger than previous theoretical estimates, putting polaritons in the strongly interacting regime.

Much of the physics of polaritons[1–13] is dominated by the fact that they have extremely light effective mass. When an exciton is mixed with a cavity photon to become an exciton–polariton, it has an effective mass about four orders of magnitude less than a vacuum electron, and about three orders of magnitude less than a typical semiconductor quantum well exciton. Therefore, one can view the exciton–polaritons, hereafter polaritons, as excitons which are given much longer diffusion lengths, with propagation distances of polaritons up to millimetres[14,15]; this may have implications for solar cells, which depend crucially on the diffusive migration of excitons[16]. Alternatively, polaritons can be viewed as photons with nonlinear interactions many orders of magnitude higher than in typical optical materials, due to their excitonic components[17]. The light effective mass of the polaritons (typically 10^{-8} that of a hydrogen atom) allows for quantum phenomena to be realized at much higher temperatures than in cold atomic gases.

Interactions among polaritons

The interaction of polaritons is presumed to come exclusively from their underlying excitonic components. These interactions renormalize the polariton dispersion, leading to a continuous blue shift to higher emission energies as the polariton density increases. To lowest order, one can view the blue shift of the polariton emission line as the real self-energy due to the interactions, and the spectral width of the polariton emission line as the imaginary self-energy arising from the same interactions. When the particles undergo Bose–Einstein condensation, the spectral width narrows due to the spontaneously emerged coherence.

Most previous theoretical works have assumed the exciton–exciton interaction strength calculated by Tassone and Yamamoto[18], found to be $g \sim 6E_b a_B^2$, where E_b is the excitonic binding energy, and a_B is the excitonic Bohr radius. Typical values for excitons in GaAs narrow quantum wells, namely $E_b \sim 10$ meV and $a_B \sim 100$ Å, give $g \sim 6\,\mu\text{eV}\,\mu\text{m}^2$. This, in turn, implies that the polariton gas is intrinsically weakly interacting, as measured by the unitless parameter $\gamma = g/(\hbar^2/2m) \sim 0.01$ (refs 19,20), using the effective mass of polaritons $m \sim 10^{-4} m_0$, where m_0 is the vacuum electron mass.

Under the mean-field approximation, at low particle density, the blue shift of ground state energy is linearly dependent on the particle density n, that is,

$$\Delta E = gn \tag{1}$$

where ΔE and n are the blue shift and particle density, respectively. In the absence of many-body correlations, the slope g is independent of the density. In the experiments reported here, we measured the energy shift ΔE of the polariton ground state at an in-plane momentum $k_\parallel = 0$ for various excitation densities. The interaction strength was then extracted as the slope of the energy shift with density.

The main difficulty in previous experiments for measuring the polariton–polariton interaction strength has been to establish the absolute density of the polaritons independent of any excitons that may be present. When the polaritons are generated by non-resonant laser excitation, not only polaritons but also bare excitons are created. This leads to a population of excitons of unknown density. If structures with short lifetime (about 2 ps) are used, the polaritons do not travel far from the cloud of excitons. Therefore, when a shift of the polariton energy is measured, it is not possible to determine how much of this shift is due to direct polariton–polariton interaction and how much is due to polariton–exciton interaction. In principle, there may also be free carriers created near the laser excitation region, which also interact with the polaritons.

[1]Department of Chemistry and Center for Excitonics, Massachusetts Institute of Technology, 77 Massachusetts Avenue, Cambridge, Massachusetts 02139, USA. [2]Department of Physics, University of Pittsburgh, 3941 O'Hara St., Pittsburgh, Pennsylvania 15218, USA. [3]Department of Electrical Engineering, Princeton University, Princeton, New Jersey 08544, USA. *e-mail: ybsun@mit.edu; snoke@pitt.edu

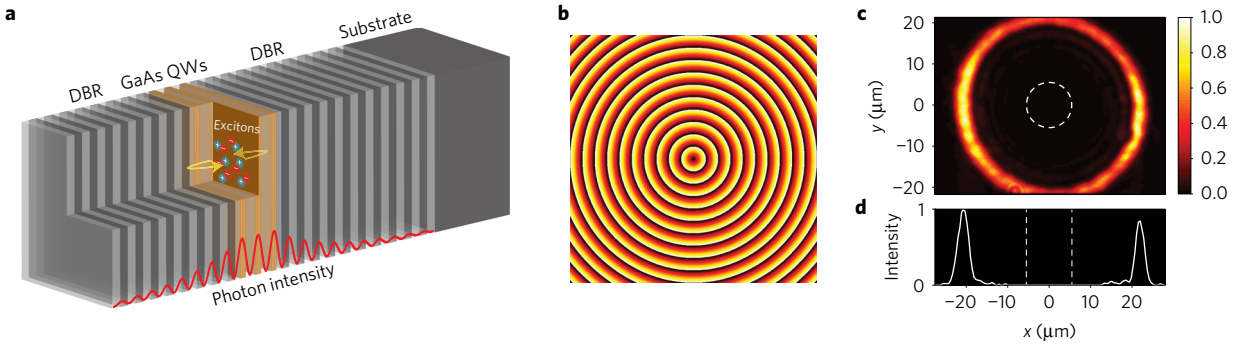

Figure 1 | Generation of an annular trap in a GaAs microcavity. a, Long-lifetime microcavity structure used in the experiment. The dark and light grey layers are the distributed Bragg reflectors (DBRs) used to confine the light. The red solid line indicates the intensity distribution of the confined cavity mode. The orange layers indicate the position of the quantum wells (QWs), with blue and red dots showing the bound electron–hole pairs (that is, excitons). The yellow arrows indicate the energy oscillation between the cavity mode and the exciton state. **b**, A representative axicon phase imprinted on the surface of the spatial light modulator used to generate the annular excitation pattern. **c**, Real-space image of the laser reflection, which is a ring with a diameter of 42 μm. The white dashed circle indicates the region where the photoluminescence (PL) is collected. **d**, The white solid line is the cross section of $y=0$ slice that is selected by the entrance of the imaging spectrometer. The white dashed lines indicate the positions of the pinhole edges.

Alternatively, if polaritons are created resonantly, they typically have a highly non-equilibrium and coherent distribution that does not allow easy extraction of the particle density.

In this work, we used a very high-Q microcavity under non-resonant excitation. The high Q implies long polariton lifetime, 200 ps or longer[15], which allows the polaritons to propagate well away from the laser excitation region[14]. By propagating polaritons to the centre of a sufficiently big optically induced annular trap, we can separate the polaritons from the population of free carriers and hot excitons. We can then extract the polariton interaction strength from the spectral data at the centre of the trap.

The interactions between polaritons are predicted to be spin-dependent, and several experiments have studied this spin dependence[21–25]. In the experiment reported here, we assume that the polaritons are equilibrated into a mixture of both spin states[1], and therefore the interaction strength we measure is an average value. Because the interaction of polaritons is stronger for spin-aligned polaritons, we expect that our measured interaction strength will be dominated by the spin-aligned contribution.

Separation of polaritons from excitation region

The sample is an $Al_{0.2}Ga_{0.8}$/AlAs $3\lambda/2$ optical cavity, with a group of four 7 nm GaAs QWs embedded at each of the three antinodes, as shown in Fig. 1a. It has a quality factor of ∼320,000 and a cavity lifetime of ∼135 ps, which is significantly higher than most samples used in earlier experiments (the lifetimes of polaritons were at most 30 ps (ref. 26), even well into excitonic detunings), confirmed by the propagation of resonantly created polaritons up to the millimetre scale[15]. The rate of radiative decay $1/\tau$ is proportional to its photonic fraction, which in turn depends on the cavity detuning δ, defined as the energy difference between the bare photon energy at $k_{\parallel}=0$ and the bare exciton energy. Because the microcavity structure used in this work is wedged, the detuning is then a function of the location on the microcavity structure. We can easily vary the detuning, and therefore the excitonic and photonic fractions of the polaritons, by performing measurements at different sample positions on the microcavity. Careful calibration of the upper and lower polariton energies as a function of position on the sample allows us to determine the detuning, and therefore the excitonic and photonic fractions of the polaritons, at each position. At the resonance of the excitons and cavity photons, the lifetime of polaritons in our sample is ∼270 ps.

During the experiment, the sample was thermally attached to a cold finger in an open-loop cryostat which was stabilized at 10 K. To accumulate polariton densities after they accelerate away from the excitation region, we made a spatial trap. We made use of the fact that excitons created by a laser field in the same structure have much larger effective mass than the polaritons; the typical polariton mass is 10^{-4} times the electron mass, while the exciton mass is of the order of a tenth of the electron mass in GaAs quantum wells. Therefore, the excitons created by a laser pulse are essentially static as seen by polaritons, and the mean-field repulsion energy of the excitons acts as a static potential energy barrier. This method has been used previously in several experiments to confine polaritons[27–30].

The annular trap in this work was formed by irradiating a spatial light modulator (SLM) with a pixel density of 1,920 × 1,080 by a continuous wave (cw) laser. The ability to address each individual pixel on the SLM allows for shaping the incident Gaussian beam into any designed intensity patterns[28–30]. We imposed an axicon phase map, shown in Fig. 1b, onto the surface of the SLM, which was placed at the Fourier plane of an imaging lens. At the conjugate plane of this lens, the Gaussian beam is transformed into a ring-shaped pattern with a diameter of ∼2 mm. With another two pairs of telescopes, a ring with a diameter in the range of 15–50 μm can be created on the sample surface, as shown in Fig. 1c. The wavelength of the cw laser was tuned to 720 nm, about 130 meV above the lower polariton resonance, to match the second reflection minimum above the stop band of the cavity at resonance. This generated a high density of free carriers along the ring. To avoid any unwanted sample heating, the cw laser was modulated by an acousto-optic modulator (AOM) at 1 kHz with a duty cycle of 0.5%.

The photoluminescence (PL) from the non-resonant excitation was collected by a microscope objective with a numerical aperture (NA) of 0.28, and was imaged in the far-field geometry to the entrance slit of a spectrometer charge-coupled device (CCD). A spatial filter was placed at a reconstructed real-space plane downstream to filter out the emission further than 5.5 μm away from the centre of the trap. The white dashed circle in Fig. 1c and the white dashed line in Fig. 1d indicate the collection region. The $y=0$ slice was selected by the spectrometer slit and then spectrally dispersed to get the emission energy. Figure 1d shows the intensity profile of the $y=0$ slice. We also measured the integrated light intensity in the collection region with and without a neutral density filter, and determined the light intensity in the collection region is ∼2,000 times smaller than that of the pumping region. This is crucial to the quality of the measurement; for, otherwise, light in the collection region can create excitons and free carriers which can lead to an additional shift of the polariton energy. As discussed in the Supplementary Information, typical energy shifts of the polaritons in the collection region are about 10% of the energy shift in the

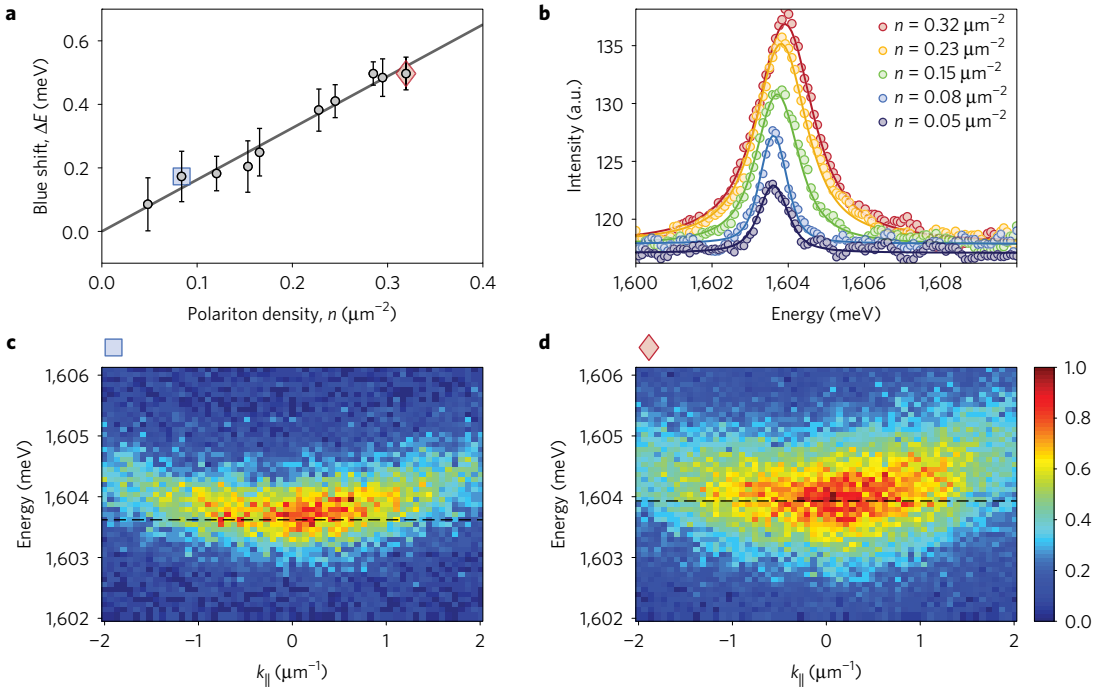

Figure 2 | Emission spectra at different polariton densities. a, Blue shift of ground state energies at different polariton densities at a detuning of $\delta = 7.70$ meV when the excitation annular profile has a diameter of 42 μm. The error bars are standard deviations of estimated energy shift. **b**, Polariton emission profiles at $k_{\parallel} = 0$ at different densities. The blue ($n = 0.08\,\mu m^{-2}$) and red ($n = 0.32\,\mu m^{-2}$) dots correspond to the densities shown as the blue square and red diamond in **a**, respectively. The solid lines are fits to Lorentzian profiles. **c**,**d**, Energy-resolved dispersions corresponding to the data points indicated by the blue square (**c**) and red diamond (**d**) in **a**, both at low density when there is no condensate. The dashed lines are the assigned energies of the ground state of polaritons. The jet colourmap is shown to calibrate the relative magnitude of the emission intensities.

pumping region. Assuming that the exciton density is proportional to the pump intensity, the energy shift of the polaritons in the collection region cannot come from the excitons.

Figure 2c shows a typical energy-resolved emission pattern in the far-field geometry (that is, angle-resolved PL, which gives the momentum distribution of the polaritons) at low excitation power, and Fig. 2d shows a case of high excitation power, but below the condensation threshold. As can be seen, the ground state of polariton energies, indicated by the horizontal dashed lines, are blue-shifted due to repulsive interactions among polaritons. As seen in Fig. 2b, there is also a Lorentzian spectral broadening, which also arises from the interactions. To a good approximation, when there is no condensate, this spectral broadening can be seen as simply the energy uncertainty given by $\Delta E = \hbar/\Delta t$, where Δt is the average incoherent scattering time. As discussed below, this broadening also gives a measure of the polariton–polariton interaction strength. At low density, the emission profile deviates away from the Lorentzian profile and resembles the Voigt profile, which accounts for the disorder broadening, as shown in Supplementary Figs 3–5.

Calibration of polariton density

Care was taken to ensure that the polaritons were nearly in spatial and thermal equilibrium. Supplementary Fig. 6 presents images of the spatial distributions of the polaritons in a trap under a similar condition, showing that the distributions are nearly spatially homogeneous. At high density, when a condensate forms, there is evidence of self-trapping into a central region of the laser-generated trap. The data reported here are for detunings with a significant exciton component, allowing good thermalization[31]. When polaritons are very photon-like, the spatial and energy profiles of the polaritons become fairly inhomogeneous in the condensate regime[32].

The greatest uncertainty in these measurements is the determination of the polariton density—that is, the total number of polaritons in the area of the field of view. We used two methods and found consistency between them. The first is to carefully determine the absolute collection efficiency of our photon detection system using photon counting, as discussed in ref. 31. The second method allowed us to set an absolute density by pegging the density at which the distribution of the polaritons is altered by the Bose–Einstein statistics of the particles. In the long-lifetime microcavity structure, polaritons are nearly in thermal equilibrium at resonance up to excitonic detunings. The equilibrium Bose–Einstein distribution is given by

$$N(E) = \frac{1}{e^{(E-\mu)/k_B T} - 1} \qquad (2)$$

At densities well below the condensation threshold, this becomes a Maxwell–Boltzmann distribution $N(E) \propto e^{-E/k_B T}$. In the quantum regime, however, when $N(E) \sim 1$ for low-energy states, the shape of the distribution is changed, and can be fitted to a value of the chemical potential μ. The value of μ controls not only the shape, but also the absolute value of $N(E)$. Therefore, we have a tight constraint on the values of μ when we fit $N(E)$ at several particle densities. By minimizing the mean-squared error in the fitting of a set of n distributions $N(E)$ collected at different pumping powers to the equilibrium Bose–Einstein model as in equation (2) with $2n+1$ free parameters, we deduce one single collection efficiency ξ as well as n temperatures and n chemical potentials for different distributions. This nominal efficiency factor was within the range of uncertainty of the number deduced from photon counting, as discussed in ref. 31.

These methods give us an accurate calibration of the polariton density in the annular trap. More generally, we do not have to rely on the details of the above calculations to get the approximate range of the polariton densities. We know that we measure the polariton spectra up to the condensation threshold (as evidenced by the sharp spectral narrowing, discussed below and also reported in ref. 33).

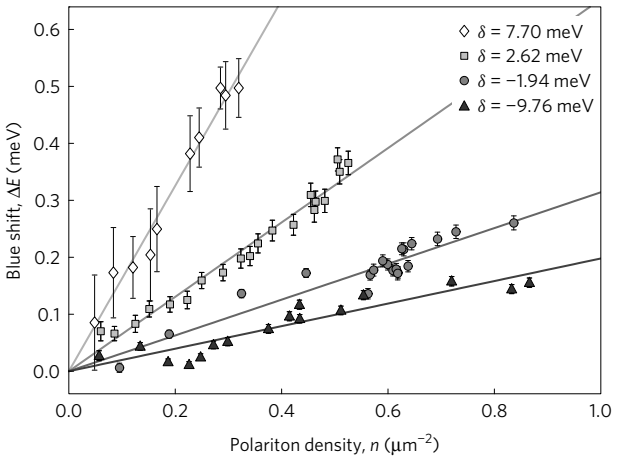

Figure 3 | Blue shifts at various detunings. Blue shifts of the ground state energies as a function of polariton density at different cavity detunings. The error bars are standard deviations of estimated energy shifts. The solid lines are fits to $\Delta E = gn$ using weighted least-squares estimates.

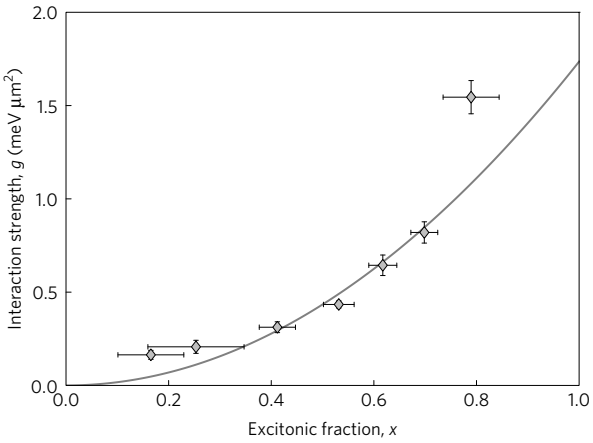

Figure 4 | Polariton–polariton interaction strength. Measured interaction strength (g) as a function of excitonic fraction (x), which is deduced for each data set from the effective mass of the lower polariton dispersion using the formula $x \simeq 1 - m_c/m_{LP}$, where m_c is the bare cavity photon mass measured at very large photonic detuning (−22.5 meV). Grey diamonds are slopes extracted from Fig. 3. The vertical and horizontal error bars represent standard deviations of the interaction strength and excitonic fraction, respectively. The solid line is a best fit to a quadratic dependence using weighted least-squares estimates.

Quantum effects will be important when the thermal de Broglie wavelength λ_{th} is comparable to the interparticle spacing r_s—that is, when

$$\lambda_{th} = \sqrt{\frac{2\pi\hbar^2}{mk_BT}} \sim r_s = n^{-1/2} \quad (3)$$

where n is the particle density and T is temperature of the particles. This implies $n \sim mk_BT/2\pi\hbar^2 \approx 4 \times 10^7\,\mathrm{cm}^{-2}$ near the condensation threshold, for $k_BT \approx 20\,\mathrm{K}$ and the polariton mass given above.

Interaction strength below condensation density

The measured number of polaritons increased linearly with pump excitation density in the low-density regime below the condensation threshold. In this range of densities, the ground state energies of the polaritons were extracted as shown in Fig. 2c,d. To determine the ground state energy at zero excitation density, we linearly extrapolate the measured blue shifts to zero density. All the blue shifts are then reported with respect to this energy. As shown in Fig. 2a, the blue shift increases linearly with the polariton density. This confirms that the interaction strength g does not depend on the density of the polaritons in this regime.

In Fig. 3, we plot the measured blue shift of the $k_\parallel = 0$ state as a function of polariton density at four representative detunings. As expected, polaritons experience higher blue shifts for excitonic detunings than for photonic detunings, since the energy renormalization presumably comes from the excitonic constituents. The solid lines show linear fits to the data using weighted least-squares estimates.

Figure 4 shows the extracted slopes at different cavity detunings versus their corresponding excitonic fractions. The interaction strength increases when excitonic fractions in polaritons are higher. The standard theory predicts that the interaction between polaritons is governed by their underlying excitonic fractions x, given by

$$x = \frac{1}{2}\left(1 + \frac{\delta}{\sqrt{\delta^2 + \Omega^2}}\right) \quad (4)$$

where Ω is the full Rabi splitting and δ is the cavity detuning, defined as $\delta = E_c(k_\parallel = 0) - E_x$, where E_c and E_x are the cavity and exciton energies, respectively. The solid line is a quadratic fit to the extracted slopes in Fig. 3. The dependence of the shift on exciton fraction is clearly superlinear, which is another indicator that the shift is not arising from polariton–exciton interactions; if interaction with excitons were the dominant cause of the blue shift, the shift would be linear with exciton fraction.

By extrapolation, the interaction strength in the limit of $x \to 1$ is determined as $1.74 \pm 0.46\,\mathrm{meV\,\mu m^2}$. This value is fairly surprising, in that it is two orders of magnitude larger than the absolute value calculated in ref. 18, which has guided many theoretical investigations of polaritons. It implies that the unitless parameter for the strength of the interactions is $\gamma = g/(\hbar^2/2m) \sim 1$, which means that the polariton gas cannot be treated by standard weakly interacting Bose gas theory. In particular, it implies that many-body correlations will play an important role at high densities.

The extrapolation to $x \to 1$ seems to imply that not only polaritons, but bare Wannier excitons also have this strong interaction. However, we note that in all the measurements here, the effective mass of the particles was very light, comparable to the polariton mass at resonance (see the Supplementary Information for a plot of the mass as a function of detuning). It may be that the strong interactions seen here depend crucially on the light effective mass of the polaritons, and therefore it may be unwarranted to extrapolate this result to the pure exciton limit.

As noted above, the polariton–polariton interactions affect not only the blue shift (real self-energy) but also the line broadening (imaginary self-energy). The Lorentzian line broadening value of $\sim$1 meV is also two orders of magnitude larger than that would be expected for the nominal exciton–exciton interaction strength. Using the semiclassical formula $\tau^{-1} = n\sigma\bar{v}$, where n is the density, $\sigma \sim a_B$ is the scattering cross section, and $\bar{v}$ is the average thermal velocity, it gives $\tau \sim 100\,\mathrm{ps}$, or $\hbar/\tau \sim 0.01\,\mathrm{meV}$ with typical values for microcavity polaritons $n = 4 \times 10^7\,\mathrm{cm}^{-2}$, $\sigma = 100\,\text{Å}$ and $\bar{v} = 2 \times 10^8\,\mathrm{cm\,s}^{-1}$ for $T = 20\,\mathrm{K}$. The measured Lorentzian broadening corresponds to a polariton–polariton scattering time of less than 1 ps.

Interaction strength above condensation density

Evidence of the importance of many-body correlations is seen in the behaviour of the blue shift at the condensation threshold. In Fig. 5, we plot the blue shift of the ground state emissions at different polariton densities up to and above the condensation threshold in an annular trap with a diameter of 36 μm, for an excitonic detuning of $\delta = 6.11\,\mathrm{meV}$. We also show the spectral width of the emission at $k_\parallel = 0$. As discussed above, the condensation threshold is indicated by spectral narrowing.

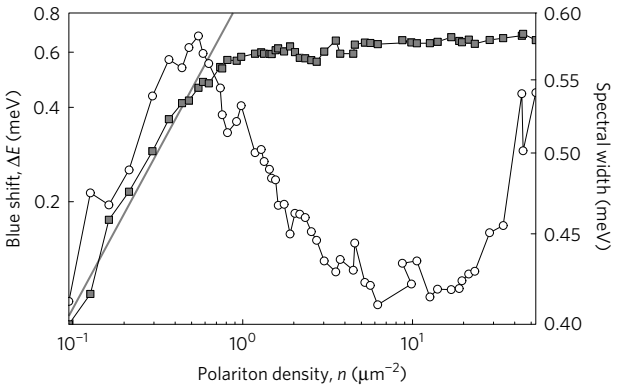

Figure 5 | Saturation of blue shift. Measured blue shift (grey squares) and spectral width (white circles) of the $k_{\|} = 0$ lower polariton emission as a function of polariton density at a cavity detuning of $\delta = 6.11$ meV in an annular trap with a diameter of 36 μm. The straight line shows a linear dependence of the blue shift in the low-density regime.

At low densities, the blue shift scales linearly as the polariton density with a slope of 0.91 ± 0.13 meV μm^2, consistent with the value expected for this detuning. The linewidth of the emission also increases linearly with density because the larger population leads to more frequent incoherent collisions, and then narrows due to the emergence of the coherence when condensation occurs. At the condensation threshold, the blue shift of the polariton emission becomes strongly sublinear with density, following a power law of $\Delta E \sim n^{0.037}$. The simple mean-field prediction for a weakly interacting Bose gas is that the shift should still be linear with density when it condenses, with an overall slope that is reduced by a factor of two due to the nature of quantum indistinguishability. The fact that the shift is strongly sublinear points to the importance of high-order correlations in the condensate regime, which have been shown to have a significant role in strongly interacting gases[34].

Implications and outlook

Given that the measured value of the blue shift is so much larger than the theoretical expectation, we consider possible ways that the measurement could be misleading. First, one may ask whether excitons and/or free carriers generated by the non-resonant laser may indeed be diffusing into the region where the polaritons are observed. We are confident that this is not the case. As the diameter of the ring trap is increased up to 50 μm, the blue shift at fixed density has a constant value independent of the trap radius (see the Supplementary Information for a plot). If exciton or free carrier diffusion were playing an important role, the blue shift at the condensate density would depend strongly on the ring radius, as their diffusion length becomes much less than the radius. Also, the exciton diffusion length has been directly measured (see, for example, ref. 10, Figure 3a therein) and is less than 10 μm. The Supplementary Information shows data for the diffusion length of the excitons. Furthermore, it is also known that the diffusion length of the polaritons decreases with increasing excitonic component, as polaritons with higher excitonic components have greater effective mass and greater interaction with phonons. This will lead to a lower exciton population far from the excitation region, while here we see that the blue shift increases with increasing excitonic fraction.

A blue shift may arise from phase-space filling, which leads to a reduction of the Rabi splitting between the upper and lower polariton branches. This is also predicted to give shifts of the order of $E_b a_B^2$ or less[35,36], much less than what we observe here. Bandgap renormalization due to heating (that is, phonon population) is known to give a red shift, not a blue shift, with increasing temperature.

Another possibility is that the polaritons generate free excitons in the centre of the trap via thermal up-conversion. In this model, excitons are present in the centre of the trap, not due to diffusion from the laser excitation region—that is, from the walls of the ring trap, but from migration of polaritons by themselves, which then turn back into free excitons by thermal excitation. For this to give the blue shift we see, assuming the standard interaction strength, there would need to be two orders of magnitude more excitons than polaritons. This would severely deplete the population of polaritons. Also, this effect should be exponentially dependent on the splitting $\Delta E_{\mathrm{split}}$ between the polariton and exciton states, due to the Boltzmann $e^{\Delta E_{\mathrm{split}}/k_B T}$ factor, but in fact we see even more blue shift than expected when the lower polaritons are very photonic, with large $\Delta E_{\mathrm{split}}$. We also see very little temperature dependence of the blue shift at constant $\Delta E_{\mathrm{split}}$ as the lattice temperature is changed.

Assuming that the above mechanisms are ruled out, we can ask what mechanism could give us much stronger effective interactions at low density than predicted. One possibility is that the nearby biexciton resonance[37] significantly affects the interactions. We believe this is not the case, because the dependence of the interaction strength on detuning is not especially strong. Another possibility is a mechanism involving disorder, which has also been invoked as a way of explaining the larger-than-expected blue shift in previous experimental results[38,39]. In our experiments, the photonic disorder is very low, but the excitonic disorder is approximately 2 meV (as measured by the inhomogeneous broadening of the bare exciton line). Jacob Taylor has suggested that disorder may cause the excitons participating in the polariton states to be spatially correlated in 'puddles' of much higher density than the average polariton density. This view requires no change to the standard exciton–exciton interaction strength. It is supported by the observation that both the blue shift and the Lorentzian line broadening are about 100 times larger than expected; both of these depend linearly on the effective density.

In conclusion, we have directly measured the polariton–polariton interaction strength by propagating polaritons to the centre of a laser-generated annular trap. The interaction strength is independent of polariton density in the low-density regime. The measured value is two orders of magnitude larger than expected from prior theoretical calculations. The polariton–polariton interaction is effectively a $\chi^{(3)}$ nonlinearity[17], and is an important parameter for the design and theoretical modelling of exciton–polaritonic optical devices. The large value measured here indicates that the efficiency of these devices may be much greater than anticipated, at least in the low-density regime. The saturation of the blue shift upon condensation calls for further theoretical analysis, and is probably due to coherent many-body effects of the condensate.

Data availability. The data that support the plots within this paper and other findings of this study are available from the corresponding author upon reasonable request.

Received 16 August 2015; accepted 21 April 2017;
published online 5 June 2017

References

1. Kasprzak, J. *et al*. Bose–Einstein condensation of exciton polaritons. *Nature* **443,** 409–414 (2006).
2. Balili, R., Hartwell, V., Snoke, D., Pfeiffer, L. & West, K. Bose–Einstein condensation of microcavity polaritons in a trap. *Science* **316,** 1007–1010 (2007).
3. Amo, A. *et al*. Superfluidity of polaritons in semiconductor microcavities. *Nat. Phys.* **5,** 805–810 (2009).
4. Lagoudakis, K. G. *et al*. Quantized vortices in an exciton–polariton condensate. *Nat. Phys.* **4,** 706–710 (2008).
5. Lagoudakis, K. G. *et al*. Observation of half-quantum vortices in an exciton–polariton condensate. *Science* **326,** 974–976 (2009).

6. Sanvitto, D. *et al*. Persistent currents and quantized vortices in a polariton superfluid. *Nat. Phys.* **6,** 527–533 (2010).
7. Nardin, G. *et al*. Hydrodynamic nucleation of quantized vortex pairs in a polariton quantum fluid. *Nat. Phys.* **7,** 635–641 (2011).
8. Tosi, G. *et al*. Geometrically locked vortex lattices in semiconductor quantum fluids. *Nat. Commun.* **3,** 1243 (2012).
9. Dreismann, A. *et al*. Coupled counterrotating polariton condensates in optically defined annular potentials. *Proc. Natl Acad. Sci. USA* **111,** 8770–8775 (2014).
10. Liu, G., Snoke, D. W., Daley, A., Pfeiffer, L. N. & West, K. A new type of half-quantum circulation in a macroscopic polariton spinor ring condensate. *Proc. Natl Acad. Sci. USA* **112,** 2676–2681 (2015).
11. Christopoulos, S. *et al*. Room-temperature polariton lasing in semiconductor microcavities. *Phys. Rev. Lett.* **98,** 126405 (2007).
12. Kena-Cohen, S. & Forrest, S. R. Room-temperature polariton lasing in an organic single-crystal microcavity. *Nat. Photon.* **4,** 371–375 (2010).
13. Plumhof, J. D., Stoferle, T., Mai, L., Scherf, U. & Mahrt, R. F. Room-temperature Bose–Einstein condensation of cavity exciton–polaritons in a polymer. *Nat. Mater.* **13,** 247–252 (2014).
14. Steger, M. *et al*. Long-range ballistic motion and coherent flow of long-lifetime polaritons. *Phys. Rev. B* **88,** 235314 (2013).
15. Steger, M., Gautham, C., Snoke, D. W., Pfeiffer, L. & West, K. Slow reflection and two-photon generation of microcavity exciton–polaritons. *Optica* **2,** 1–5 (2015).
16. Zhugayevych, A. & Tretiak, S. Theoretical description of structural and electronic properties of organic photovoltaic materials. *Annu. Rev. Phys. Chem.* **66,** 305–330 (2015).
17. Snoke, D. in *Exciton–Polaritons in Microcavities* Vol. 172 (eds Timofeev, V. & Sanvitto, D.) (Springer Series in Solid State Sciences, Springer, 2012).
18. Tassone, F. & Yamamoto, Y. Exciton–exciton scattering dynamics in a semiconductor microcavity and stimulated scattering into polaritons. *Phys. Rev. B* **59,** 10830–10842 (1999).
19. Prokof'ev, N., Ruebenacker, O. & Svistunov, B. Critical point of a weakly interacting two-dimensional Bose gas. *Phys. Rev. Lett.* **87,** 270402 (2001).
20. Prokof'ev, N. & Svistunov, B. Two-dimensional weakly interacting Bose gas in the fluctuation region. *Phys. Rev. A* **66,** 043608 (2002).
21. Amo, A. *et al*. Exciton–polariton spin switches. *Nat. Photon.* **4,** 361–366 (2010).
22. Antón, C. *et al*. Optical control of spin textures in quasi-one-dimensional polariton condensates. *Phys. Rev. B* **91,** 075305 (2015).
23. Sich, M. *et al*. Effects of spin-dependent interactions on polarization of bright polariton solitons. *Phys. Rev. Lett.* **112,** 046403 (2014).
24. Sekretenko, A. V., Gavrilov, S. S. & Kulakovskii, V. D. Polariton–polariton interactions in microcavities under a resonant 10 to 100 picosecond pulse excitation. *Phys. Rev. B* **88,** 195302 (2013).
25. Takemura, N., Trebaol, S., Wouters, M., Portella-Oberli, M. T. & Deveaud-Pledran, B. Heterodyne spectroscopy of polariton spinor interactions. *Phys. Rev. B* **90,** 195307 (2014).
26. Wertz, E. *et al*. Spontaneous formation and optical manipulation of extended polariton condensates. *Nat. Phys.* **6,** 860–864 (2010).
27. Tosi, G. *et al*. Sculpting oscillators with light within a nonlinear quantum fluid. *Nat. Phys.* **8,** 190–194 (2012).
28. Cristofolini, P. *et al*. Optical superfluid phase transitions and trapping of polariton condensates. *Phys. Rev. Lett.* **110,** 186403 (2013).
29. Askitopoulos, A. *et al*. Polariton condensation in an optically induced two-dimensional potential. *Phys. Rev. B* **88,** 041308 (2013).
30. Askitopoulos, A. *et al*. Robust platform for engineering pure-quantum-state transitions in polariton condensates. *Phys. Rev. B* **92,** 035305 (2015).
31. Sun, Y. *et al*. Bose–Einstein condensation of long-lifetime polaritons in thermal equilibrium. *Phys. Rev. Lett.* **118,** 016602 (2017).
32. Sun, Y. *et al*. Stable switching among high-order modes in polariton condensates. Preprint at http://arXiv.org/abs/1602.03024 (2016).
33. Nelsen, B. *et al*. Dissipationless flow and sharp threshold of a polariton condensate with long lifetime. *Phys. Rev. X* **3,** 041015 (2013).
34. Zimmermann, R. Dynamical T-matrix theory for high-density excitons in coupled quantum wells. *Phys. Stat. Solidi. b* **243,** 2358–2362 (2006).
35. Ciuti, C., Savona, V. & Quattropani, A. Role of the exchange of carriers in elastic exciton–exciton scattering in quantum wells. *Phys. Rev. B* **58,** 7926 (1998).
36. Pavlovic, G. *Exciton–Polaritons in Low Dimensional Structures* PhD thesis, Université Blaise Pascal - Clermont-Ferrand (2010).
37. Takemura, N., Trebaol, S., Wouters, M., Portella-Oberli, M. T. & Deveaud, B. Polaritonic feshbach resonance. *Nat. Phys.* **10,** 500–504 (2014).
38. Marchetti, F. M., Keeling, J., Szymańska, M. H. & Littlewood, P. B. Thermodynamics and excitations of condensed polaritons in disordered microcavities. *Phys. Rev. Lett.* **96,** 066405 (2006).
39. Marchetti, F. M., Keeling, J., Szymańska, M. H. & Littlewood, P. B. Absorption, photoluminescence, and resonant Rayleigh scattering probes of condensed microcavity polaritons. *Phys. Rev. B* **76,** 115326 (2007).

Acknowledgements

We thank A. Daley and D. Pekker for fruitful discussions and J. Beaumarriage for assistance in the calibration of the detuning map of the sample. Y.S., Y.Y. and K.A.N. were supported as part of the Center for Excitonics, an Energy Frontier Research Center funded by the US Department of Energy, Office of Science, Office of Basic Energy Sciences under Award Number DE-SC0001088. M.S., G.L. and D.W.S. were supported by the National Science Foundation under grants PHY-1205762 and DMR-1104383. L.N.P. and K.W. were funded by the Gordon and Betty Moore Foundation through the EPiQS initiative Grant GBMF4420, and by the National Science Foundation MRSEC Grant DMR-1420541.

Author contributions

Y.S. and D.W.S. designed the experiments; Y.S. performed the experiment; Y.S. and D.W.S. analysed the data; Y.S., Y.Y. and M.S. calibrated the detuning map of the sample; L.N.P. and K.W. grew the microcavity structure; all the authors participated in the discussion of the results and manuscript preparation.

Additional information

Supplementary information is available in the online version of the paper. Reprints and permissions information is available online at www.nature.com/reprints. Publisher's note: Springer Nature remains neutral with regard to jurisdictional claims in published maps and institutional affiliations. Correspondence and requests for materials should be addressed to Y.S. or D.W.S.

Competing financial interests

The authors declare no competing financial interests.